Crosstalk between three-dimensional plasmonic slot waveguides

Georgios Veronis and Shanhui Fan

Department of Electrical Engineering, Stanford University, Stanford, California 94305

shanhui@stanford.edu

Abstract: We investigate in detail the crosstalk between plasmonic slot waveguides. We show that the coupling behavior of deep subwavelength three-dimensional (3-D) plasmonic slot waveguides is very different from the one of two-dimensional (2-D) metal-dielectric-metal (MDM) plasmonic waveguides. While in the 2-D case the coupling occurs only through the metal, in the 3-D case the coupling occurs primarily through the dielectric, in which the evanescent tail is much larger compared to the one in the metal. Thus, in most cases the coupling between 3-D plasmonic slot waveguides is much stronger than the coupling between the corresponding 2-D MDM plasmonic waveguides. Such strong coupling can be exploited to form directional couplers using plasmonic slot waveguides. On the other hand, with appropriate design, the crosstalk between 3-D plasmonic slot waveguides can be reduced even *below* the crosstalk levels of 2-D MDM plasmonic waveguides, without significantly affecting their modal size and attenuation length. Thus, 3-D plasmonic slot waveguides can be used for ultradense integration of optoelectronic components.

References and links

1. W. L. Barnes, A. Dereux, and T. W. Ebbesen, "Surface plasmon subwavelength optics," Nature **424,** 824–830 (2003).
2. J. Takahara, S. Yamagishi, H. Taki, A. Morimoto, and T. Kobayashi, "Guiding of a one-dimensional optical beam with nanometer diameter," Opt. Lett. **22,** 475–477 (1997).
3. J. C. Weeber, A. Dereux, C. Girard, J. R. Krenn, and J. P. Goudonnet, "Plasmon polaritons of metallic nanowires for controlling submicron propagation of light," Phys. Rev. B **60,** 9061–9068 (1999).
4. J. R. Krenn, B. Lamprecht, H. Ditlbacher, G. Schider, M. Salerno, A. Leitner, and F. R. Aussenegg, "Non-diffraction-limited light transport by gold nanowires," Europhys. Lett. **60,** 663–669 (2002).
5. M. L. Brongersma, J. W. Hartman, and H. A. Atwater, "Electromagnetic energy transfer and switching in nanoparticle chain arrays below the diffraction limit," Phys. Rev. B **62,** R16356–R16359 (2000).
6. S. A. Maier, P. G. Kik, H. A. Atwater, S. Meltzer, E. Harel, B. E. Koel, and A. A. G. Requicha, "Local detection of electromagnetic energy transport below the diffraction limit in metal nanoparticle plasmon waveguides," Nat. Mater. **2,** 229–232 (2003).
7. S. I. Bozhevolnyi, V. S. Volkov, E. Devaux, and T. W. Ebbesen, "Channel plasmon-polariton guiding by sub-wavelength metal grooves," Phys. Rev. Lett. **95,** 046802 (2005).
8. S. I. Bozhevolnyi, V. S. Volkov, E. Devaux, J. Y. Laluet, and T. W. Ebbesen, "Channel plasmon subwavelength waveguide components including interferometers and ring resonators," Nature **440,** 508–511 (2006).
9. R. Zia, M. D. Selker, P. B. Catrysse, and M. L. Brongersma, "Geometries and materials for subwavelength surface plasmon modes," J. Opt. Soc. Am. A **21,** 2442–2446 (2004).
10. K. Tanaka and M. Tanaka, "Simulations of nanometric optical circuits based on surface plasmon polariton gap waveguide," Appl. Phys. Lett. **82,** 1158–1160 (2003).

11. F. Kusunoki, T. Yotsuya, J. Takahara, and T. Kobayashi, "Propagation properties of guided waves in index-guided two-dimensional optical waveguides," Appl. Phys. Lett. **86,** 211101 (2005).

12. G. Veronis and S. Fan, "Guided subwavelength plasmonic mode supported by a slot in a thin metal film," Opt. Lett. **30,** 3359–3361 (2005).

13. L. Liu, Z. Han, and S. He, "Novel surface plasmon waveguide for high integration," Opt. Express **13,** 6645-6650 (2005).

14. D. F. P. Pile, T. Ogawa, D. K. Gramotnev, Y. Matsuzaki, K. C. Vernon, K. Yamaguchi, T. Okamoto, M. Haraguchi, and M. Fukui, "Two-dimensionally localized modes of a nanoscale gap plasmon waveguide," Appl. Phys. Lett. **87,** 261114 (2005).

15. E. Feigenbaum and M. Orenstein, "Modeling of complementary (Void) plasmon waveguiding," J. Lightwave Technol. **25,** 2547–2562 (2007).

16. D. M. Pozar, *Microwave Engineering*, (Wiley, New York, 1998).

17. N. N. Feng, M. L. Brongersma, and L. Dal Negro, "Metal-dielectric slot-waveguide structures for the propagation of surface plasmon polaritons at 1.55 μm," IEEE J. Quantum Electron. **43,** 479–485 (2007).

18. G. Veronis and S. Fan, "Modes of subwavelength plasmonic slot waveguides," J. Lightwave Technol. **25,** 2511–2521 (2007).

19. A. Yariv and P. Yeh, *Photonics: Optical Electronics in Modern Communications*, (Oxford University Press, New York, 2006).

20. J. A. Pereda, A. Vegas, and A. Prieto, "An improved compact 2D full-wave FDFD method for general guided wave structures," Microwave Opt. Technol. Lett. **38,** 331–335 (2003).

21. J. Jin, *The Finite Element Method in Electromagnetics*, (Wiley, New York, 2002).

22. S. J. Al-Bader, "Optical transmission on metallic wires - fundamental modes," IEEE J. Quantum Electron. **40,** 325–329 (2004).

23. E. D. Palik, *Handbook of Optical Constants of Solids*, (Academic, New York, 1985).

24. H. J. Hagemann, W. Gudat, and C. Kunz, "Optical constants from the far infrared to the x-ray region: Mg, Al, Cu, Ag, Au, Bi, C, and Al_2O_3," J. Opt. Soc. Am. **65,** 742–744 (1975).

25. G. Veronis and S. Fan, "Bends and splitters in metal-dielectric-metal subwavelength plasmonic waveguides," Appl. Phys. Lett. **87,** 131102 (2005).

1. Introduction

The capability of guiding light at deep subwavelength scales is of great interest in optoelectronics, in part because such capability may enable ultradense integration of optoelectronic circuits [1]. This prospect for integration has motivated significant recent activities in exploring plasmonic waveguide structures [2, 3, 4, 5, 6, 7, 8, 9, 10, 11, 12, 13, 14, 15]. Among these, two-conductor waveguide geometries, which are the optical analogue of microwave transmission lines [16], are of particular interest because they support modes at deep subwavelength scale with high group velocity over very wide range of frequencies. As a prominent example of two-conductor waveguide geometries, three-dimensional (3-D) plasmonic slot waveguides, consisting of a deep subwavelength slot introduced in a thin metallic film, were recently investigated [12, 13, 14, 17, 18].

To enable ultradense integration, however, a key consideration is the packing density of optical waveguides and devices. When two waveguides are brought in close proximity, their modes overlap resulting in coupling and crosstalk between the waveguides [19]. The crosstalk, in general, becomes stronger as the distance between the waveguides is reduced. Thus, the coupling strength between two waveguides sets a limit on their maximum packing density. It is therefore important to investigate the crosstalk between subwavelength plasmonic slot waveguides. In previous studies, Zia et al. [9] investigated the coupling between two-dimensional (2-D) metal-dielectric-metal (MDM) plasmonic waveguides. They showed that such waveguides can be put at a distance of ~150 nm without significant crosstalk. In addition, Liu et al. [13] investigated the coupling between 3-D plasmonic slot waveguides formed on the same thin metal film.

In this paper we investigate in detail the crosstalk between plasmonic slot waveguides. We first show that for coupled lossy waveguides in general there is a maximum in the power transfer efficiency from one waveguide to the other. This maximum transfer efficiency is determined by the ratio of the coupling length between the two waveguides to their mean attenuation length.

We then consider the coupling between symmetric plasmonic slot waveguides formed on the same thin metal film. We show that the coupling behavior of deep subwavelength 3-D plasmonic slot waveguides is very different from the one of corresponding 2-D MDM plasmonic waveguides. While in the 2-D case the coupling occurs only through the metal, in the 3-D case the coupling occurs primarily through the dielectric, in which the evanescent tail is much larger compared to the one in the metal. Thus, the coupling between 3-D plasmonic slot waveguides is much stronger than the coupling between the corresponding 2-D MDM plasmonic waveguides. Such a strong coupling can be used to form a directional coupler using slot waveguides. For coupling between asymmetric plasmonic slot waveguides, as well as for vertically-coupled plasmonic slot waveguides which are formed on parallel thin metal films, we also find that the coupling through the dielectric is dominant. On the other hand, we show that, by modifying the metal regions between the two slots, the crosstalk between 3-D plasmonic slot waveguides can be reduced even *below* the crosstalk levels of 2-D MDM plasmonic waveguides. Examples include a structure in which the metal film separating the two slots has an increased thickness, as well as a structure in which the metal region separating the two slots is *I*-shaped. We show that both of these structures greatly reduce the crosstalk between the plasmonic slot waveguides, without significantly affecting their modal size and attenuation length. Thus, with appropriate design, plasmonic slot waveguides can be used for ultradense integration of optoelectronic components.

The remainder of this paper is organized as follows. In Section 2 we provide a general analysis of the coupling between lossy waveguides. In Section 3 we describe the simulation methods used for the analysis of the coupled plasmonic waveguides. In Section 4 we investigate various cases of coupling between plasmonic slot waveguides. In Section 5 we propose and analyze structures which reduce the crosstalk between plasmonic slot waveguides. Finally, our conclusions are summarized in Section 6.

2. Coupling between lossy waveguides

Since a key goal in this paper is to evaluate crosstalk and to develop ways to suppress it, we will be considering the coupler formed between two identical waveguides such that phase-matching is automatically satisfied. This corresponds to the strongest coupling [19], and therefore the worst-case scenario for crosstalk. Thus, we start from a single-mode waveguide structure, and consider a coupler structure consisting of two such waveguides, which satisfies the mirror symmetry relation $\varepsilon_r(x,y) = \varepsilon_r(-x,y)$, where ε_r is the dielectric function. We assume that the waveguide is uniform along the z direction. Such a coupler supports two eigenmodes with either symmetric ($\mathbf{E}_s(x,y)$) or antisymmetric ($\mathbf{E}_a(x,y)$) electric field distribution with respect to the y axis. Due to the mirror symmetry of the structure, the two modes are orthogonal, i.e.,

$$\int \frac{1}{2}\mathrm{Re}[\mathbf{E}_\nu \times \mathbf{H}_\mu^* \cdot \hat{z}]dS = \delta_{\nu\mu}, \ \ \nu,\mu = s,a,$$

where $\mathbf{H}_s(x,y)$ ($\mathbf{H}_a(x,y)$) is the magnetic field of the symmetric (antisymmetric) mode. The total electric field is given by

$$\mathbf{E}(x,y,z) = c_s(z)\mathbf{E}_s(x,y) + c_a(z)\mathbf{E}_a(x,y), \tag{1}$$

where the modal field amplitudes $c_s(z)$, $c_a(z)$ are given by $c_s(z) = c_s(0)\exp(-\gamma_s z)$, $c_a(z) = c_a(0)\exp(-\gamma_a z)$, and the modal propagation constants γ_s, γ_a are in general complex, i.e., $\gamma_s = \alpha_s + i\beta_s$, $\gamma_a = \alpha_a + i\beta_a$. The properties of the eigenmodes of the coupler completely determine the transfer behavior between the waveguides. To see this, we define the electric field distributions

$$\mathbf{E}_l(x,y) \equiv \mathbf{E}_s(x,y)/\sqrt{2} + \mathbf{E}_a(x,y)/\sqrt{2}, \tag{2}$$

$$\mathbf{E}_r(x,y) \equiv \mathbf{E}_s(x,y)/\sqrt{2} - \mathbf{E}_a(x,y)/\sqrt{2}, \tag{3}$$

which are highly concentrated either on the left ($\mathbf{E}_l(x,y)$) or on the right ($\mathbf{E}_r(x,y)$) waveguide. Note that the left and right field distributions in Eqs. (2) and (3) are also orthogonal to each other. For weakly-coupled waveguides these field distributions are almost identical to the field distribution of an isolated waveguide. The total electric field in Eq. (1) can then also be written as

$$\mathbf{E}(x,y,z) = c_l(z)\mathbf{E}_l(x,y) + c_r(z)\mathbf{E}_r(x,y). \tag{4}$$

Using Eqs. (1)-(4) we obtain

$$\begin{bmatrix} c_l(z) \\ c_r(z) \end{bmatrix} = \begin{bmatrix} \frac{1}{\sqrt{2}} & \frac{1}{\sqrt{2}} \\ \frac{1}{\sqrt{2}} & -\frac{1}{\sqrt{2}} \end{bmatrix} \begin{bmatrix} c_s(z) \\ c_a(z) \end{bmatrix}, \tag{5}$$

and

$$|c_l(z)|^2 + |c_r(z)|^2 = |c_s(z)|^2 + |c_a(z)|^2.$$

We now consider the case where only $\mathbf{E}_l(x,y)$, which is highly concentrated on the left waveguide, is excited at $z = 0$, i.e. $c_l(0) = 1$, $c_r(0) = 0$. Using Eq. (5), the power coupled into the right field distribution after a distance L is evaluated to be

$$|c_r(L)|^2 = |\frac{1}{2}[\exp(-\gamma_s L) - \exp(-\gamma_a L)]|^2. \tag{6}$$

For lossless waveguides, i.e. $\gamma_s = i\beta_s$, $\gamma_a = i\beta_a$, using Eq. (6), we obtain

$$|c_r(L)|^2 = \sin^2(\frac{\beta_s - \beta_a}{2}L) = \sin^2(\frac{\pi}{2}\frac{L}{L_c}),$$

where we defined the coupling length as

$$L_c \equiv \pi/|\beta_s - \beta_a|. \tag{7}$$

We observe that, in the case of coupled lossless waveguides, power is transferred completely from the left to the right waveguide for a distance L equal to the coupling length L_c. Thus, in order to limit the crosstalk between two adjacent lossless waveguides, we must have $L \ll L_c$.

We now consider coupled lossy waveguides. Using Eq. (6) we obtain

$$|c_r(L)|^2 = \exp(-2\frac{L}{\overline{L}_p})|\frac{1}{2}[\exp(-\gamma_- L) - \exp(\gamma_- L)]|^2, \tag{8}$$

where $\overline{L}_p \equiv 2/(\alpha_s + \alpha_a)$ is the mean attenuation length, and $\gamma_- = (\alpha_s - \alpha_a)/2 + i(\beta_s - \beta_a)/2$. Eq. (8) suggests that, unlike lossless waveguides, for coupled lossy waveguides complete transfer of power from one waveguide to the other is not possible, since loss is always present during the transfer process. Instead, for coupled lossy waveguides there is a maximum in power coupled from one waveguide to the other:

$$p_{\max} \equiv \max_L |c_r(L)|^2. \tag{9}$$

As it turned out, for the structures considered in this paper $|\alpha_s - \alpha_a|/2 \ll |\beta_s - \beta_a|/2$, so that

$$\gamma_- \simeq i(\beta_s - \beta_a)/2. \tag{10}$$

We found that in all cases considered in this paper, the approximation of Eq. (10) results in less than 1% error in the calculated maximum transfer power p_{max}. Inserting Eq. (10) into Eq. (8) we obtain

$$|c_r(L)|^2 \simeq \exp(-2\frac{L}{\overline{L}_p})\sin^2(\frac{\pi}{2}\frac{L}{L_c}),$$

and

$$p_{max} \simeq \frac{\exp(-2x\arctan(x^{-1}))}{1+x^2}, \ \ x = 2L_c/(\pi\overline{L}_p). \tag{11}$$

Therefore, under the approximation of Eq. (10), the maximum transfer power p_{max} is only a function of $L_c/\overline{L}_p$ (Fig. 1). When the coupling length L_c is much smaller than the mean attenuation length $\overline{L}_p$, the maximum transfer power approaches 1, similar to the lossless case. In the opposite limit, when the coupling length L_c is much larger than the mean attenuation length $\overline{L}_p$, the maximum transfer power approaches 0 (Fig. 1). In this case, there is almost no power coupled from one waveguide to the other, irrespective of L. In addition, since there is almost no coupling between the waveguides, the power in each waveguide attenuates with the attenuation length of an individual plasmonic slot waveguide.
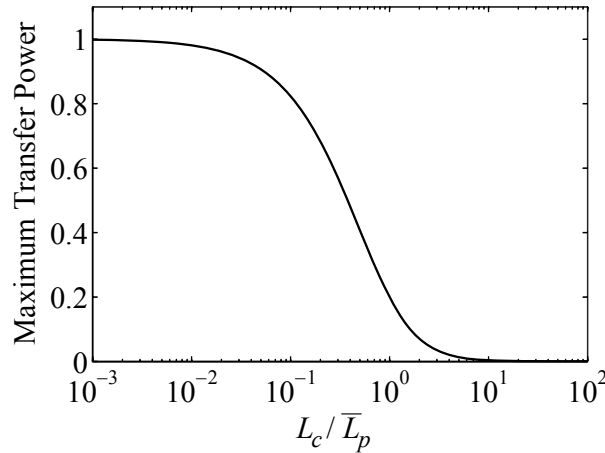

Fig. 1. Maximum transfer power p_{max} as a function of $L_c/\overline{L}_p$, under the approximation $\gamma_- \simeq i(\beta_s - \beta_a)/2$ (see Section 2). Here L_c is the coupling length, and $\overline{L}_p$ is the mean attenuation length. In all cases considered in this paper, this approximation results in less than 1% error in the calculated p_{max}.

We would like to emphasize that the above analysis is *exact*, as long as the propagation constants of the eigenmodes γ_s and γ_a are known. Therefore, in this paper we will employ numerical methods to evaluate γ_s and γ_a directly, and from these we will determine the coupling behavior.

3. Simulation method

We use a full-vectorial finite-difference frequency-domain (FDFD) mode solver [20, 12] to cal-culate the symmetric ($\mathbf{E}_s(x,y)$, $\mathbf{H}_s(x,y)$), and the antisymmetric ($\mathbf{E}_a(x,y)$, $\mathbf{H}_a(x,y)$) eigenmodes of coupled waveguides (Sec. 2), and the corresponding modal propagation constants γ_s and γ_a at a given wavelength λ_0. For waveguiding structures which are uniform in the z direction, if an $\exp(-\gamma z)$ dependence is assumed for all field components, Maxwell's equations reduce to two

coupled equations for the transverse magnetic field components H_x and H_y [20]. These equations are discretized on a non-uniform orthogonal grid resulting in a sparse matrix eigenvalue problem of the form $\mathbf{Ah} = \gamma^2 \mathbf{h}$, which is solved using iterative sparse eigenvalue techniques [21]. The discretization scheme is based on Yee's lattice [20]. To calculate the bound eigenmodes of the coupled waveguides, we ensure that the size of the computational domain is large enough so that the fields are negligibly small at its boundaries [22], while for leaky modes we use perfectly matched layer absorbing boundary conditions [21]. An important feature of this formulation is the absence of spurious modes [22]. In addition, the frequency-domain mode solver allows us to directly use experimental data for the frequency-dependent dielectric constant of metals [23, 24], including both the real and imaginary parts, with no approximation. Once the modal propagation constants γ_s and γ_a are calculated, the coupling length L_c between the two plasmonic slot waveguides is calculated using Eq. (7), and the maximum transfer power $p_{\max}$ using Eqs. (8) and (9).

4. Coupling between plasmonic slot waveguides

Using the analytic theory in Section 2 and the numerical methods in Section 3, we consider coupling between deep subwavelength plasmonic slot waveguides. We focus on the optical communication wavelength ($\lambda_0 = 1.55$ μm), where subwavelength plasmonic slot waveguides have attenuation lengths of tens of micrometers [12, 18]. Our reference structure is a symmetric plasmonic slot waveguide [18] consisting of a slot of width $w = 50$ nm in a silver film of thickness $h = 50$ nm embedded in silica ($n_s = 1.44$).

We first consider the coupling between two such symmetric plasmonic slot waveguides which are formed on the same thin silver film (Fig. 2(b)). In general, the coupling length L_c decreases as the distance D between the slots decreases (Fig. 2(e)). The presence of the left slot imposes a dielectric perturbation on the propagation of the bound mode of the right plasmonic slot waveguide and vice versa. It can be shown that, for weak coupling, the coupling length L_c between two waveguides is inversely proportional to the overlap integral of their field profiles in the perturbed region [19]. In the case of plasmonic slot waveguides formed on the same metal film, L_c will therefore be inversely proportional to the modal field amplitude of the plasmonic slot waveguide on the adjacent slot. Since far from the slot the modal field amplitude decays asymptotically as $\sim \exp(-\alpha\rho)/\sqrt{\rho}$, where $\alpha = \mathrm{Re}\sqrt{-\gamma^2 - (\frac{2\pi n_s}{\lambda_0})^2}$ [12], the coupling length L_c will increase with D as $\sim \sqrt{D}\exp(\alpha D)$. We have indeed verified that this is the case for $D > 200$ nm, where the coupling between the waveguides is weak.

In Fig. 2(f) we show the maximum transfer power $p_{\max}$ between the two plasmonic slot waveguides as a function of D (Fig. 2(b)). As expected, $p_{\max}$ decreases as D increases. For $D > 0.94$ μm we have $p_{\max} < 10^{-3}$, so that the crosstalk between the two plasmonic waveguides is negligible. As mentioned above, $p_{\max}$ is a function of the ratio of the coupling length L_c to the mean attenuation length $\overline{L}_p$ (Eq. (11)). In the weak coupling regime ($D > 200$ nm) the mean attenuation length $\overline{L}_p$ of the modes supported by the structure is insensitive to D, since the fraction of the optical power in the metal is not affected by the coupling. Thus, in this regime $p_{\max}$ is solely determined by L_c.

In the strong coupling regime ($D < 200$ nm) the coupling length is in the order of a few microns (Fig. 2(e)), and the maximum transfer power $p_{\max}$ approaches 1 (Fig. 2(f)). In this regime, the structure of Fig. 2(b) can be used as a directional coupler to perform power division, power coupling and switching [19]. In the strong coupling regime, as D decreases, there is an increase in the fraction of the modal power in the metal region separating the two slots for the mode with symmetric electric field distribution ($\mathbf{E}_s(x,y)$). Consequently, the attenuation length of this mode decreases significantly as D is decreased. This results in decreased mean attenuation
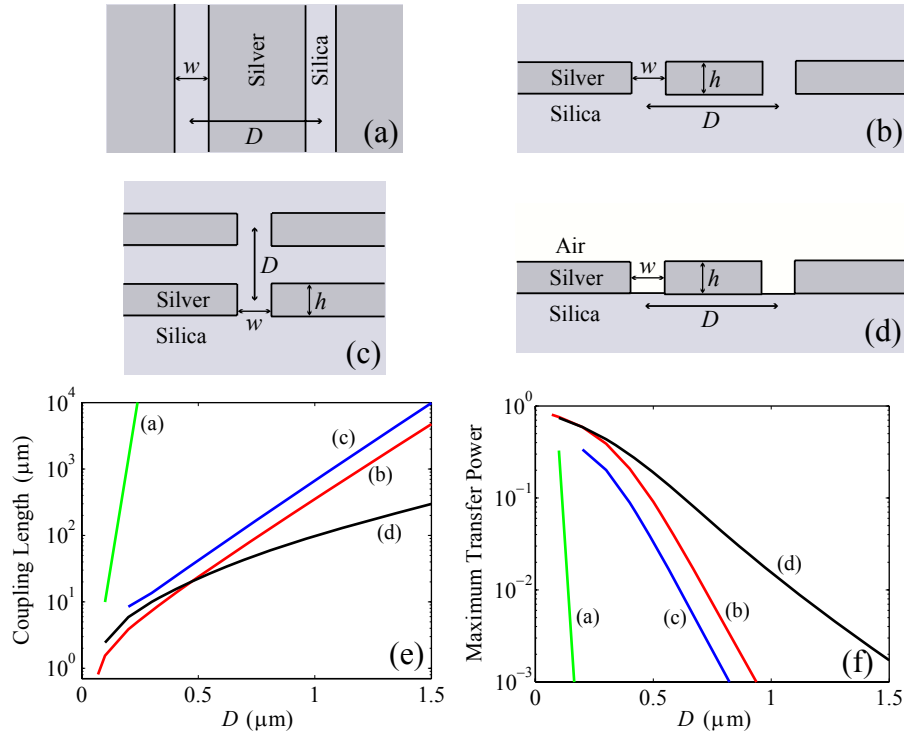
Fig. 2. (a) Schematic of two coupled 2-D MDM plasmonic waveguides. (b) Schematic of two coupled symmetric plasmonic slot waveguides which are formed on the same thin metal film. (c) Schematic of two vertically-coupled symmetric plasmonic slot waveguides which are formed on parallel thin metal films. (d) Schematic of two coupled asymmetric plasmonic slot waveguides which are formed on the same thin metal film. (e) Coupling length L_c as a function of the distance D between two coupled plasmonic waveguides. Results are shown for 2-D MDM plasmonic waveguides (green line), symmetric plasmonic slot waveguides formed on the same metal film (red line), vertically-coupled symmetric plasmonic slot waveguides formed on parallel metal films (blue line), and asymmetric plasmonic slot waveguides formed on the same metal film (black line). In all cases, the slot widths are $w = 50$ nm, the metal film thicknesses are $h = 50$ nm, and the operating wavelength is $\lambda_0 = 1.55$ μm. (f) Maximum transfer power p_{max} as a function of the distance D between two coupled plasmonic waveguides. All other parameters are as in (e).

length $\overline{L}_p$ and faster decay of the total power in the system of coupled slot waveguides when compared with an isolated waveguide. In addition, in this regime the behavior of the coupling strength with respect to the distance D cannot be inferred directly from the field profile of an isolated plasmonic slot waveguide.

In the strong coupling regime the coupler can be used for power division. However, we note that an alternative way to perform power division is to use a splitter. Such a device is extremely compact and has almost zero splitting loss [25].

The behavior of coupling in 3-D plasmonic slot waveguides turns out to be completely different from the one of the corresponding 2-D MDM plasmonic waveguides. In Figs. 2(e) and 2(f) we also show L_c and p_{max}, respectively, for a corresponding 2-D MDM plasmonic waveguide coupler with the same dielectric layer width w (Fig. 2(a)). We observe that for the coupled 3-D plasmonic slot waveguides, L_c is order of magnitudes smaller, and p_{max} is order of magnitude

larger than the quantities of the corresponding 2-D MDM plasmonic waveguides. For example, a minimum distance of $D_{min} =0.16\,\mu$m between 2-D MDM plasmonic waveguides is sufficient to maintain negligible crosstalk ($p_{max} < 10^{-3}$), while for 3-D plasmonic slot waveguides the corresponding minimum distance is $D_{min} =0.94\,\mu$m (Fig. 2(f)). We emphasize that, while in the 2-D case the coupling occurs only through the metal, in the 3-D case the coupling occurs primarily through the dielectric, in which the evanescent tail is much larger compared to the one in the metal.

We also note that, as $h \to \infty$, the modal propagation constant of a 3-D plasmonic slot waveguide approaches asymptotically the modal propagation constant of the corresponding 2-D MDM plasmonic waveguide ($\lim\limits_{h\to\infty} \gamma_{3D}(h) = \gamma_{2D}$) [18]. Similar asymptotic behavior is observed in the coupling length L_c and the maximum transfer power p_{max} between 3-D plasmonic slot waveguides ($\lim\limits_{h\to\infty} L_{c,3D}(h) = L_{c,2D}$ and $\lim\limits_{h\to\infty} p_{max,3D}(h) = p_{max,2D}$). However, while the modal characteristics of 3-D plasmonic slot waveguides converge fast to the corresponding characteristics of 2-D MDM waveguides ($\gamma_{3D}(h = 100nm) \simeq \gamma_{2D}$) [18], in the case of coupled 3-D plasmonic slot waveguides, the convergence of $L_{c,3D}(h)$ and $p_{max,3D}(h)$ to the corresponding 2-D MDM quantities $L_{c,2D}$ and $p_{max,2D}$ is much slower and does not occur until $h >1\mu$m. This is again due to the fact that the coupling through the dielectric is much stronger than the coupling through the metal, so that only when the metal film becomes quite thick does the coupling through the dielectric become negligible.

Since the coupling in 3-D plasmonic slot waveguides occurs primarily through the dielectric, the asymptotic behavior of vertically-coupled structures (Fig. 2(c)) is very similar to that of horizontally-coupled structures (Fig. 2(b)). The coupling length L_c for the vertically-coupled waveguides also increases with D as $\sim \sqrt{D}\exp(\alpha D)$ for $D >200$ nm (Fig. 2(e)), since far from the slot the modal field amplitude decays asymptotically as $\sim \exp(-\alpha\rho)/\sqrt{\rho}$ in both the horizontal and vertical directions [12]. In addition, in the weak coupling regime ($D >200$ nm) the dependence of the maximum transfer power p_{max} on D for the vertically-coupled plasmonic slot waveguides is similar to the one of horizontally-coupled waveguides (Fig. 2(e)). There are, on the other hand, some differences between these two systems. In general, the coupling is stronger for horizontally-coupled plasmonic slot waveguides, since, for a given distance D, the modal field amplitude is larger in the horizontal than in the vertical direction. In addition, for $D <200$ nm the modes of the vertically-coupled plasmonic slot waveguides leak into one of the modes of the dielectric-metal-dielectric-metal-dielectric (DMDMD) structure formed by the two parallel metal films. Thus, the vertically-coupled slot waveguides cannot be used as an efficient directional coupler, since the leakage of power to the modes of the corresponding DMDMD structure eliminates the guiding.

In Figs. 2(e) and 2(f) we also show the coupling length L_c and maximum transfer power p_{max}, respectively, between two asymmetric plasmonic slot waveguides [18] formed on the same thin silver film (Fig. 2(d)). Each waveguide consists of an air slot in the silver film which is deposited on silica. Since $n_s =1.44>1$, the field decay rate is larger in air [12]. Thus, in the case of coupled asymmetric plasmonic slot waveguides, the coupling occurs primarily through the dielectric substrate. In addition, since $n_s =1.44>1$, the effective index of the mode of an asymmetric plasmonic slot waveguide is lower than the effective index of the mode of the corresponding symmetric plasmonic slot waveguide [18]. Thus, the field decay rate in the far field of the slot ($D >500$ nm) is smaller in the asymmetric case, resulting in stronger coupling (Figs. 2(e), and 2(f)). Note also that in the strong coupling regime the mode with antisymmetric electric field distribution ($\mathbf{E}_a(x,y)$) may become leaky into the substrate. More specifically, if the mode of the asymmetric slot waveguide with width $2w$ and height h is leaky, then for the coupled asymmetric slot waveguides of width w and height h (Fig. 2(d)) there exists a cutoff distance D_{cutoff} below which the antisymmetric mode becomes leaky.
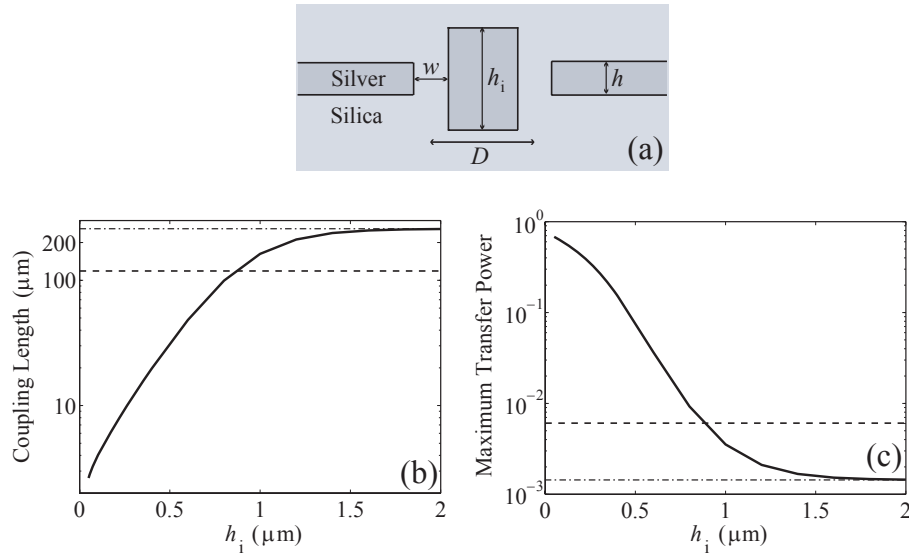
Fig. 3. (a) Schematic of a structure consisting of two coupled plasmonic slot waveguides, in which the metal film separating the two slots has an increased thickness h_i. (b) Coupling length L_c as a function of h_i (solid line). The distance between the two plasmonic slot waveguides is $D =150$ nm. All other parameters are as in Fig. 2(e). Also shown are the asymptotic value of L_c for $h_i \rightarrow \infty$ (dash-dotted line), and L_c for two coupled 2-D MDM plasmonic waveguides with the same w and D (dashed line). (c) Maximum transfer power p_{max} as a function of h_i (solid line). Also shown are the asymptotic value of p_{max} for $h_i \rightarrow \infty$ (dash-dotted line), and p_{max} for two coupled 2-D MDM plasmonic waveguides with the same w and D (dashed line). All other parameters are as in (b).

5. Reducing crosstalk between plasmonic slot waveguides

In the previous section we saw that the coupling behavior of deep subwavelength 3-D plasmonic slot waveguides is very different from that of 2-D MDM plasmonic waveguides, and the minimum distance required for negligible crosstalk is therefore much larger in the 3-D case. Here we show that, with appropriate design, the crosstalk between deep subwavelength 3-D plasmonic slot waveguides can be reduced even *below* the crosstalk levels of 2-D MDM plasmonic waveguides.

As a starting point, to reduce the coupling through the dielectric, we increase the thickness h_i of the metal film separating the two slots (Fig. 3(a)). We observe that as h_i increases, the coupling strength between the slots decreases, so that L_c increases (Fig. 3(b)), and p_{max} decreases (Fig. 3(c)). As $h_i \rightarrow \infty$, both L_c and p_{max} approach constant values. In addition, for $h_i > 0.9$ μm, we have $L_{c,3D}(h_i) > L_{c,2D}$ and $p_{max,3D}(h_i) < p_{max,2D}$, i.e. the crosstalk between 3-D plasmonic slot waveguides is reduced below the crosstalk levels of the corresponding 2-D MDM plasmonic waveguides. The use of a thicker metal region in the center provides two effects that help to suppress the crosstalk. First, the thicker metal film removes part of the dielectric between the slots. Since the field decays much slower in the dielectric compared to the metal, the dielectric region between the slots should be most critical to the coupling. Therefore, replacing the dielectric between the slots by metal greatly reduces the crosstalk. Second, the use of a thicker metal film breaks the local symmetry in each individual slot. As a result, compared with the mode in an individual slot (Fig. 4(a)), the mode in the coupler is actually pushed away from the central metal region (Fig. 4(b)). (Similar modal pattern is also observed in plasmonic strip

waveguides [18].) Consequently, the coupling between 3-D plasmonic slot waveguides can be even weaker compared with the coupling between the corresponding 2-D MDM structures.

The crosstalk between the waveguides can be further reduced by using an *I*-shaped central metal region (Fig. 5(a)), which further reduces the coupling through the dielectric. In Figs. 5(b) and 5(c) we show the coupling length L_c and maximum transfer power p_{max}, respectively, between the two plasmonic slot waveguides as a function of w_i (Fig. 5(a)). We observe that, for a given thickness h_i, as w_i increases, the coupling strength between the slots decreases, so that L_c increases (Fig. 5(b)), and p_{max} decreases (Fig. 5(c)). As $w_i \rightarrow \infty$, both L_c and p_{max} approach constant values. In addition, we observe that the additional metal films do not significantly modify the modal power density profile (Figs. 4(b), 4(c)). We also found that the presence of the additional metal films modifies the attenuation length of the supported modes by only $\sim 1\%$. In other words, the *I*-shaped metal region further reduces the crosstalk between the plasmonic slot waveguides, without significantly affecting their modal size and attenuation length.
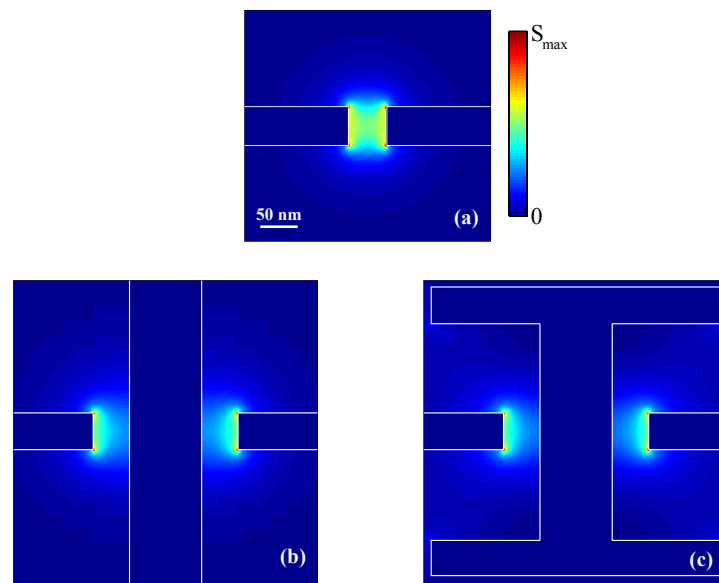

Fig. 4. (a) Power density profile of the fundamental mode of a symmetric plasmonic slot waveguide consisting of a slot of width $w = 50$ nm in a silver film of thickness $h = 50$ nm embedded in silica ($n_s = 1.44$). (b) Power density profile of the mode with symmetric electric field distribution ($\mathbf{E}_s(x,y)$), supported by the structure of Fig. 3(a) for $h_i = 1$ μm. All other parameters are as in Fig. 3(b). Since the coupling between the two plasmonic slot waveguides is negligible for $h_i = 1$ μm (Figs. 3(b), 3(c)), the power density profiles of the symmetric ($\mathbf{E}_s(x,y)$) and antisymmetric ($\mathbf{E}_a(x,y)$) modes are almost identical. (c) Power density profile of the mode with symmetric electric field distribution ($\mathbf{E}_s(x,y)$), supported by the structure of Fig. 5(a) for $w_i = 150$ nm. All other parameters are as in Fig. 5(b). Since the coupling between the two plasmonic slot waveguides is negligible for $w_i = 150$ nm (Figs. 5(b), 5(c)), the power density profiles of the symmetric ($\mathbf{E}_s(x,y)$) and antisymmetric ($\mathbf{E}_a(x,y)$) modes are almost identical.

We also note that, even though the dimensions of the *I*-shaped metal region ($\sim$400 nm) are not deep subwavelength, the lengthscale of interest is the distance D (pitch) between the slots. Thus, with appropriate design, plasmonic slot waveguides can be very densely packed

in a planar plasmonic integrated optical circuit with a pitch of only ∼150 nm. In addition, the proposed geometries consist of a number of interconnected metal regions. We note that the current electronic integrated circuit technology already uses nanoscale metallic structures as interconnects. It should therefore be possible to fabricate the proposed geometries with CMOS-compatible fabrication techniques, using lithography and etching processes.
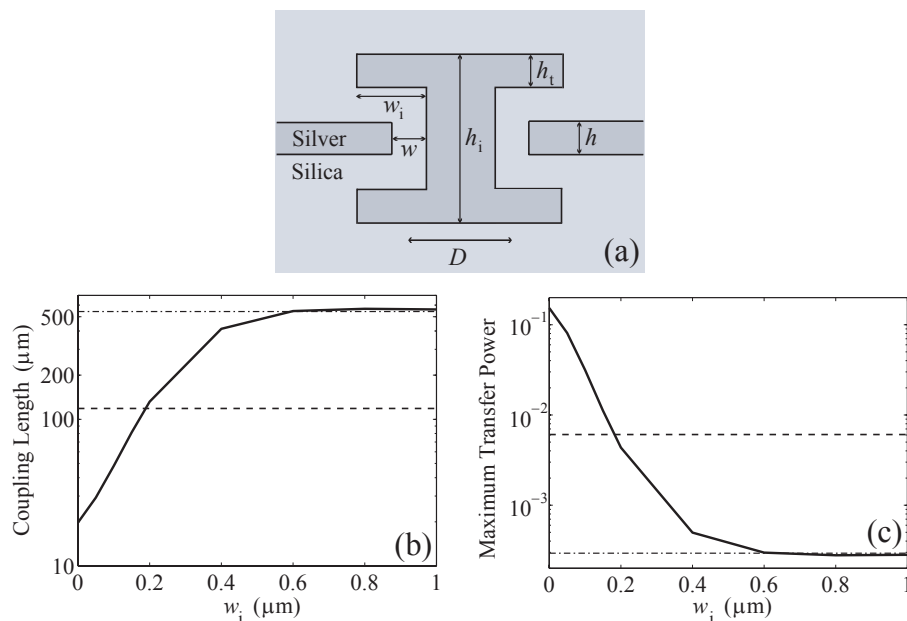

Fig. 5. (a) Schematic of a structure consisting of two coupled plasmonic slot waveguides, in which the metal region separating the two slots is *I*-shaped, and includes two additional metal films of thickness h_t. (b) Coupling length L_c as a function of w_i (solid line). The metal film thicknesses are h_i =400 nm, h_t =50 nm. All other parameters are as in Fig. 3(b). Also shown are the asymptotic value of L_c for $w_i \rightarrow \infty$ (dash-dotted line), and L_c for two coupled 2-D MDM plasmonic waveguides with the same w and D (dashed line). (c) Maximum transfer power p_{max} as a function of w_i (solid line). Also shown are the asymptotic value of p_{max} for $w_i \rightarrow \infty$ (dash-dotted line), and p_{max} for two coupled 2-D MDM plasmonic waveguides with the same w and D (dashed line). All other parameters are as in (b).

6. Summary

In this paper we first showed that for coupled lossy waveguides in general there is a maximum in the power transfer efficiency from one waveguide to the other. This maximum transfer efficiency depends on the ratio of the coupling length between the two waveguides to their mean attenuation length.

We then investigated in detail the crosstalk between plasmonic slot waveguides. We calculated the eigenmodes of coupled plasmonic waveguides at a given wavelength using a full-vectorial FDFD mode solver. We first considered the coupling between symmetric 3-D plasmonic slot waveguides formed on the same thin metal film. We showed that the coupling behavior of deep subwavelength 3-D plasmonic slot waveguides is very different from the one of corresponding 2-D MDM plasmonic waveguides. While in the 2-D case the coupling occurs only through the metal, in the 3-D case the coupling occurs primarily through the dielectric,

in which the evanescent tail is much larger compared to the one in the metal. Thus, the coupling between 3-D plasmonic slot waveguides is much stronger than the coupling between the corresponding 2-D MDM plasmonic waveguides. Such a strong coupling can be used to form a directional coupler using slot waveguides, to perform power division, power coupling and switching.

We also considered the coupling between asymmetric plasmonic slot waveguides, as well as vertically-coupled plasmonic slot waveguides which are formed on parallel thin metal films. In the case of coupled asymmetric plasmonic slot waveguides, the coupling occurs primarily through the dielectric substrate. In addition, the field decay rate in the far field of the slot is smaller in the asymmetric case, resulting in stronger coupling compared to the symmetric case.

Finally, we showed that, by modifying the metal regions between the two slots, the crosstalk between 3-D plasmonic slot waveguides can be reduced even *below* the crosstalk levels of 2-D MDM plasmonic waveguides. Examples include a structure in which the metal film separating the two slots has an increased thickness, as well as a structure in which the metal region separating the two slots is *I*-shaped. We showed that both of these structures greatly reduce the crosstalk between the plasmonic slot waveguides, without significantly affecting their modal size and attenuation length. Thus, with appropriate design, plasmonic slot waveguides can be used for ultradense integration of optoelectronic components.

Acknowledgments